Electrochemical Impedance Study of PEM Fuel Cells. Experimental Diagnostics and Modeling of Air Cathodes

Mariana Ciureanu* and Raymond Roberge

H Power Enterprises of Canada, Inc., 1068 Bégin, Ville St. Laurent, Québec, Canada H4R1V8

Received: September 13, 2000; In Final Form: January 31, 2001

The impedance response of a H_2/air PEM FC was investigated in conditions relevant for the operation of low-power fuel cells, used for portable applications (cell temperature close to ambient and moderate humidification). The dependence of EIS pattern on cell voltage, humidification temperature, and air flow rate was examined systematically. The spectrum of the air cathode at room temperature was found to contain two arcs, the potential dependence of which was analyzed in terms of the flooded-agglomerate model for gas diffusion electrodes. The high-frequency (HF) loop is responsible for processes occurring in the cathode catalyst layer: interfacial charge transfer and mass transport of air in the pores of the catalyst layer (agglomerate diffusion) and in the Nafion layer surrounding the catalyst particles (thin film diffusion). On the basis of its flow rate dependence, the low-frequency loop (LF) was assigned to the mass transport limitation which appears in the backing due to liquid water accumulation. The model equations lead to excellent fits to experimental data and enable evaluating data of practical significance—exchange current and Tafel plot slope, as well as the parameters characterizing agglomerate and thin-film diffusion. The individual overpotential losses due to kinetic, ohmic, and the three types of mass transport limitations were estimated in a typical case. The results were used to interpret the dependence of spectra on operating parameters: air flow rate, type and temperature of humidification. Also, the electrochemically active surface area of the electrocatalyst was evaluated from double layer capacitances.

Introduction

Proton exchange membrane fuel cells (PEMFC) are promising power sources, since they offer a highly efficient and environmentally friendly solution for energy conversion. These devices have attracted considerable research effort in recent years, aimed at providing a better understanding of the factors which may affect their performance: electrode composition and structure; membrane characteristics; operating parameters (cell temperature, humidification, gas composition, pressure). Among those studies, a special place is occupied by transient methods and electrochemical impedance spectroscopy (EIS), which, in principle, are able to provide more information than the steady-state experiments.[1−6] The main advantage of EIS as a diagnostic tool for discussing fuel cell behavior is the capacity to resolve in the frequency domain the individual contributions of the various factors in determining the overall PEM FC power losses—ohmic, kinetic, and mass transport.[1] Such a separation provides useful information both for the optimization of the fuel cell design and the selection of most appropriate operating conditions.[1,7,8]

EIS spectra of H_2/O_2 PEM FC are practically entirely determined by the cathode, which is the main contributor to overpotential losses. The response of the impedance to the polarization of the cathode was the object of several theoretical treatments. The most complete description of the behavior of porous gas diffusion electrodes (GDE) was the thin-film-flooded agglomerate model.[9,10] In this model, the cathode catalyst layer, present at the surface of an electrochemically inert substrate, is considered to contain agglomerated zones with a thickness L_y, filled with electrolyte and covered at the outside with a thin layer of pure electrolyte (of thickness δ). The agglomerates are intercalated with open hydrophobic channels through which the oxidant reaches the thin film at the surface of the flooded pores, dissolves, and diffuses to the catalyst particles, where the faradaic step occurs. The "agglomerate effect" appears because, as oxygen diffuses into the open hydrophobic pore, it is depleted progressively, thus creating a concentration gradient along the pore. The thin film diffusion effects are the consequence of the appearance of a concentration gradient in the thin electrolyte layer which covers the walls of the flooded pore. The flooded agglomerate model has provided a successful approach for the interpretation of the steady-state behavior of fuel cells[12−16], but has received relatively little attention for discussing impedance results. According to the flooded-agglomerate model, the impedance pattern of a gas diffusion cathode should present three loops:[10] a loop at the highest frequency, due to the double layer charging through the charge transfer resistance; a mid-frequency arc, caused by the agglomerate dynamics; an arc at lowest frequency, due to diffusion of oxygen through the thin film. However, in practice, the existence of those three impedance loops was never evidenced experimentally, probably due to a superposition of the time scales of the three processes. In most experimental EIS studies on PEM fuel cells, only one impedance arc was observed[7,8] and little information was provided on the relative contribution of the charge transfer and diffusional effects. There are only a few papers which provide evidence of the presence of two loops in EI spectra obtained at high overpotentials. The low-frequency (LF) loop appears to be most interesting, since it may provide information on a diffusional processes responsible for an important part of the total resistance. However, the origin of this loop is controversial: the loop was assigned to the slow diffusion of oxygen

10.1021/jp003273p CCC: $20.00 © 2001 American Chemical Society
Published on Web 04/07/2001

through the backing,[1] back diffusion of water in the membrane,[2] or diffusion of water in the catalyst layer.[3]

The purpose of the present paper is to reexamine those problems, in an attempt to provide information on the relative contributions of ohmic, kinetic, and diffusional effects on the impedance response. Also, a special emphasis will be on the effect of humidification and air stoichiometry, which have received little attention by this technique. Unlike most experimental studies reported to date, which were conducted at relatively high temperatures (cell temperature 70−80 °C, humidification temperature 90−105 °C), our studies were concerned with examining the behavior in mild conditions (cell temperature 25 °C; moderate humidification or no humidification at all). Data thus obtained provide information relevant for the functioning of low-power fuel cells, as those currently used for portable applications.

Another consequence of working in mild conditions is the possibility to get more information on the cathode "flooding", which, according to our data, should be regarded as the main cause which limits the performance of the cell at high overpotentials.

At low cell temperatures, the cell currents are low and differential resistances are high; this enables performing experiments with cells having large surface areas, similar with those actually employed in power devices. Unlike low surface area cells (1 cm^2 or less), where wicking effects at the backing edges prevent cathode flooding, large surface cells are particularly affected by this process, which considerably reduces the cell performance.

Experimental Section

The fuel cell tested was a single cell with a geometric surface area of 25 cm^2 employing Nafion 113.5 polymer electrolyte membrane. The electrodes consisted of a thin-film catalyst layer with 1.7 mg of Pt/cm^2 , pressed on a Teflonized gas-diffusion backing of Toray paper. The catalyst layer was obtained by spraying onto the backing an ink containing a Pt catalyst and a diluted solution containing Nafion and Teflon (1% and 0.4%, respectively). The EMA was obtained by pressing the electrodes with the Nafion at 280 F. The gas distribution plates and graphite bipolar plates were taken from a small power fuel cell. The average electrochemically active surface area of the same electrode was determined by cyclic voltammetry as described in our previous work[5] and was found to be 200 cm^2/cm^2.

The electrodes were supplied with pure hydrogen (the anode) and air (the cathode) at atmospheric pressure. Previous EIS experiments[5] made in both two- and three-electrode arrangement demonstrated that the cell impedance is determined overwhelmingly by the cathode. Therefore, all measurements reported in this paper were made in a two electrode arrangement, with the anode serving both as auxiliary and reference electrode. The cathode potential was evaluated by adding the ohmic drop IR to the experimental cell voltage $V_{cath} = E_{cell} + IR$, and the cathodic overpotential was calculated as $\eta_c = |V_{cath} - E_o|$, where E_o is the open circuit potential.

The cell was operated at 25 °C, and the gas streams were humidified at various temperatures in the 30−60 °C range. The gas flows and humidification were controlled with a test station manufactured by Fuel Cell Technologies Inc.

The ac impedance spectra were recorded using a Schlumberger 1250 frequency-response analyzer, controlled by a PAR 273A potentiostat−galvanostat (EG&G Instruments Corp.). The impedance spectra were measured in the constant-voltage mode by sweeping frequencies over the 0.015 Hz−65 kHz range and recording 10 points/decade. The modulating voltage was 15 mV. To minimize contact resistances, measurements were made in a four-probe arrangement. The impedance spectrum in the high-frequency range shows an inductive behavior, characteristic to the experimental setup. Such inductive characteristics have been reported by other authors in impedance studies on batteries and fuel cells.[17] To avoid complications resulting from these characteristics, we have limited the high-frequency range to 1 kHz.

Typically, a dc polarization curve was recorded prior to impedance measurements, to determine the dc current corresponding to each cell voltage and to calculate the *IR*-corrected voltage. The constancy of the current measured before and after the impedance measurements was taken as a criterion for the stability of the cell during the experiment.

The bias voltage was changed in the range 1.00−0.65 V, which is the operational potential range characteristic for low-power fuel cells. The gas flows (16 sccm for hydrogen and 40 sccm for air) were selected to be higher (by a factor of 1.2 and 2.0) than the stoichiometric amounts evaluated from the dc current at 0.6 V in the conditions of the experiment (25 °C, hydrogen and air at atmospheric pressure). These flows were maintained constant throughout the experiments over the entire investigated potential range, unless otherwise stated.

Results

General Pattern of the EI Spectra. The impedance spectrum measured at several cell voltages is presented in Figure 1a,b. From Figure 1a it may be seen that at high cell voltages (low cathode overpotential) the spectrum typically consists of a single depressed semicircle, with the high-frequency (HF) intercept, R_Ω and a diameter R_p.

With decreasing voltage, R_p decreases first rather rapidly (Figure 1a). As the cell potentials decreases below 0.75 V (Figure 1b), this loop first becomes almost constant and then starts increasing. In the same potential range, a second loop appears, the diameter of which (R_d) increases with decreasing cell potentials. As seen from the Bode plots presented in Figure 2a, this new loop is centered in the low-frequency (LF) range, with characteristic frequencies between 0.065 and 0.1 Hz.

The characteristic frequencies of the first loop (Figure 2a) increase with decreasing potential, while remaining lower than those found by other authors.[1] The difference was expected, in view of the particular experimental conditions selected — operating temperature (25 °C) and atmospheric pressures for hydrogen and oxygen. As seen from Figure 2b, the increase of the cell temperature from 25 to 73 °C results in a high-frequency shift of the main maximum in the Bode plot by one order of magnitude. At the same time, as a result of this temperature increase, the LF maximum practically disappears.

NLSQ Fitting. The general pattern of the impedance plots in Figures 1b and 2 suggests a system with two time constants. Therefore, a simple equivalent circuit containing a series of two parallel *RC* circuits was used to fit the EI spectra in Figure 1b using a NLSQ procedure, as presented in Scheme 1a. Here, R_Ω is the ohmic resistance of the electrochemical cell plus contacts, which can be determined from the high-frequency limit of the resistance. The other components of the circuit account only for the cathode. In the simplest approximation, C_1 stands for the capacity of the double layer, R_1 for the charge-transfer resistance and R_2 and C_2 for a diffusional process in the LF range. More sophisticated forms of the equivalent circuit could be imagined, to account for the existence of several types of

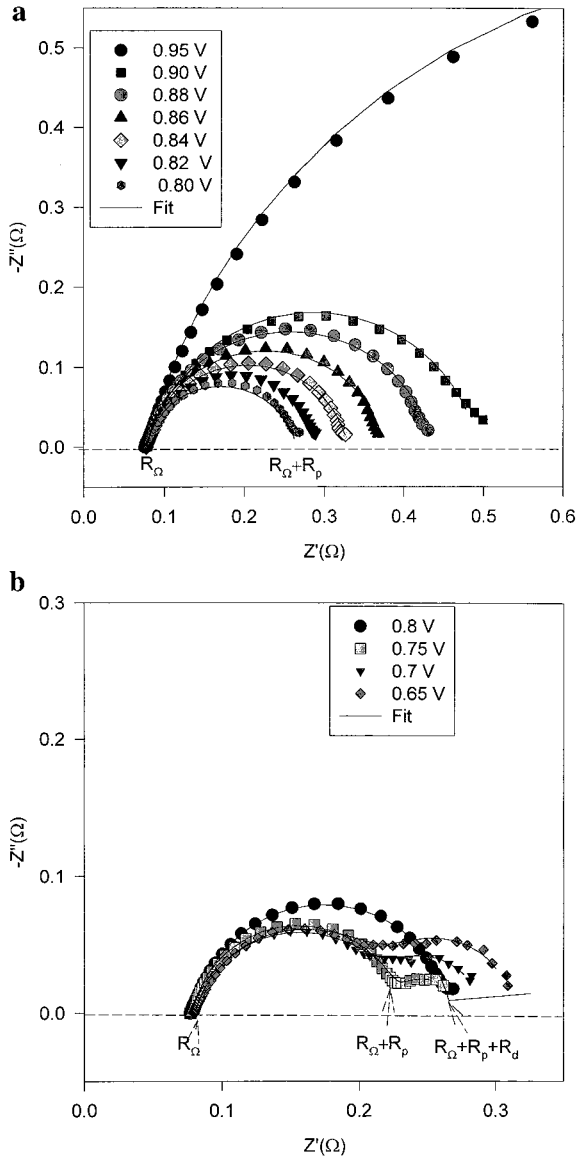

Figure 1. (a) Potential dependence of the Nyquist plots in the range 0.9−0.8 V. $t_{cell} = 25$ °C, $v_{H_2}/v_{air} = 16$ sccm/40 sccm, and $t_{H_2}/t_{air} = 40$ °C/40 °C. The legend specifies the bias potential. (b) Potential dependence of the Nyquist plots in the range 0.8−0.65 V. The experimental conditions are the same as in (a).

diffusion processes. However, since in such cases, there are obvious ambiguities in the assignment of the calculated components, we did not choose this option.

The impedance spectra in Figure 1b could be fitted by the nonlinear least-squares procedure (NLSQ) using the equivalent circuit in Scheme 1a, but the quality of the fit was relatively poor. On the contrary, if C_1 was substituted by the corresponding constant phase element T_1, as in Scheme 1b, the fit was perfect, as can be observed by the comparison between experimental data (points) and the fitted curves (continuous lines). For the spectra with one loop only, as in Figure 1a, the equivalent circuit used contained only the series combination of R_Ω and (R_1, T_1), as in Scheme 1c. T_1 is a constant phase element, which introduces an impedance given by

$$Z_{CPE} = 1/[T_1(j\omega)^{\varphi}] \quad (1)$$

where $\varphi \leq 1$ is a constant. The distributed capacitive term T_1 becomes coincident with the corresponding capacitance C_1 when $\varphi = 1$.

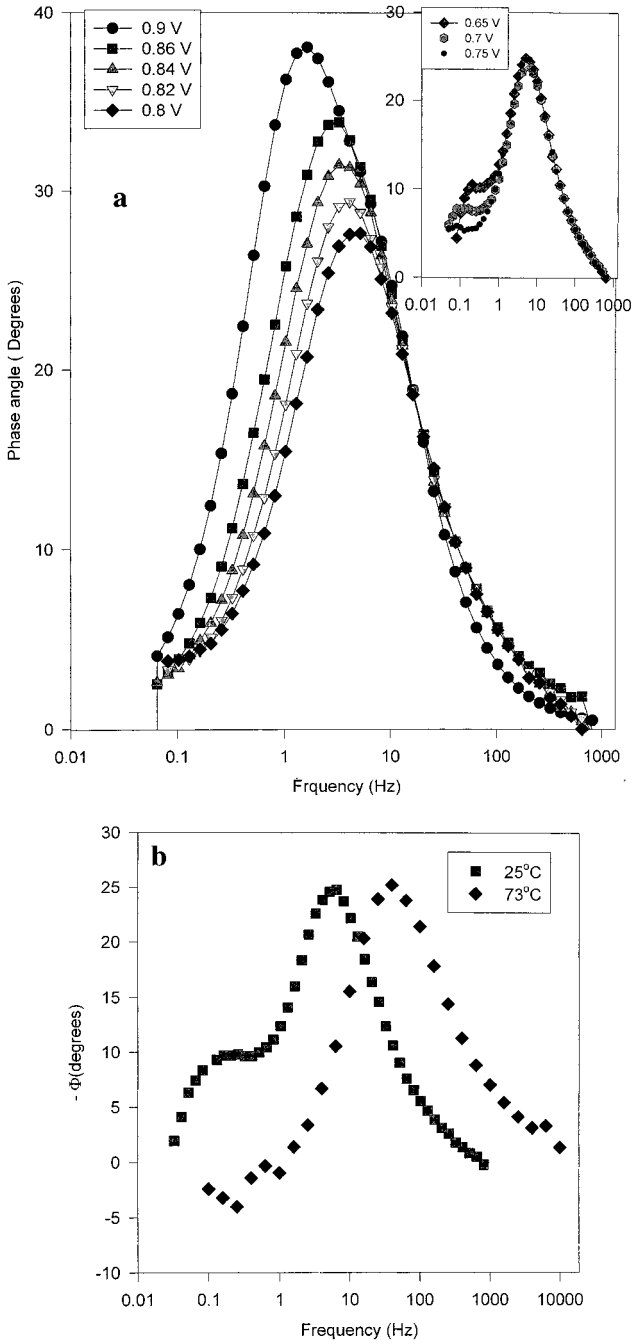

Figure 2. (a) Potential dependence of the Bode plots. The experimental conditions are the same as in Figure 1a,b. The legend specifies the bias potential. (b) Temperature dependence of the Bode plots at 0.65 V. The legend specifies cell temperature. Humidification temperatures (for hydrogen and air) were higher by 10 °C than t_{cell}.

The physical reason for replacing C_1 by T_1 results from the fact that, in a porous electrode, the capacitance due to the double layer charging is distributed along the length of the pores. Therefore, at very low frequencies, when the current penetrates almost to the end of pores, the total capacitance is that of an electrode with an "unfolded" surface, corresponding to the total surface area of the pores (or to an important part of it).[10] At higher frequencies, the current penetrates the pore to a depth depending on frequency and the surface area decreases. To account for this special behavior of porous electrodes, several models have been suggested, including the replacement of the circuit with distributed capacitances by the simple circuits of Scheme 1c. Fitting the experimental data with the equivalent

SCHEME 1

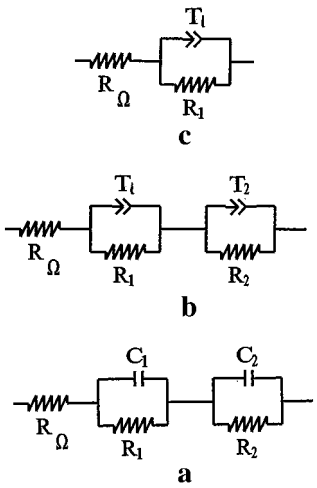

circuits in Scheme 1b,c resulted in practically constant values of $\varphi = 0.85 \pm 0.02$ for experiments performed at cell potentials between 0.95 and 0.65 V. This constancy suggests that there is no change in the current penetration depth in the potential range under investigation. Also, this enables comparisons between experimental values obtained in rather different experimental conditions.

From the values of T_1 the double layer capacitance may be calculated as described in ref 18:

$$C_1^{\varphi} = T_1/(R_\Omega^{-1} + R_1^{-1})^{1-\varphi} \quad (2)$$

The values thus obtained (Table 1) may be used to estimate the electrochemically active surface area of the electrode, by dividing the value by the capacitance of 1 cm^2 of Pt in liquid electrolytes at 0.9 V vs NHE, i.e $C_{dl}^{o} = 40\ \mu F/cm^2$.[19] The value thus obtained, 399 cm^2/cm^2, is higher, but of the same order of magnitude than that obtained from cyclic voltammetry experiments.[5] Since the catalyst contains Pt black, this value is due preponderantly to Pt, with eventual minor contributions from carbon. As the values of C_{dl}^{o} recommended in the literature are scattered between 3 and 60 $\mu F/cm^2$,[20] the consistency may be regarded as acceptable. For example, using the latter value, one obtains an electrochemically active area of 260 cm^2/cm^2.

Ohmic Resistance of the Membrane. The resistance R_Ω represents the total ohmic resistance of the cell and can be expressed as a sum of contributions from uncompensated contact resistance R_c and ohmic resistances of the cell components: the ohmic resistance of the membrane R_m, of the catalyst layer R_{cat}, of the backing R_{bac}, and of the end plates R_{ep} and that of the contacts between the membrane/catalyst layer, catalyst layer/backing, and backing/end plates. Among those terms, R_m and $R_{m/cat}$ are ionic resistances, while the remaining terms are electronic resistances:

$$R_\Omega = R_c + (R_m + R_{cat} + R_{back} + R_{ep} + R_{m/cat} + R_{cat/back} + R_{back/ep}) = R_c + R_s \quad (3)$$

The exact contribution of those terms is difficult to establish. The terms in parentheses (R_s), among which R_m is the main contributor, are inversely proportional with the surface area of the cell, so that in single cells with large surface areas they make a relatively small contribution to R_Ω. Our experiments, performed with different humidification conditions, showed practically constant values for R_Ω at $0.078 \pm 0.002\ \Omega$. To separe R_s from R_c, we have performed experiments with small stacks containing different number (N) of identical cells. The value of $R_\Omega = R_c + N^*R_s$ was represented as a function of N. The slope of the straight line thus obtained provided R_s. The value thus obtained is $R_s = 0.0075\ \Omega$; for a surface area of 1 cm^2 this corresponds to $0.18\ \Omega\ cm^2$, a result reasonably close to previous estimates of Nafion membrane resistance by other authors.[21] The fact that, in our single cell experiments, R_m represents about 10% of R_Ω explains why changes in the working conditions resulted only in small absolute changes in R_Ω . In stack experiments, where the relative contribution of R_s to R_Ω is much higher, changes of R_Ω with conditions causing membrane dehydration were clearly observed.[22]

Analysis of the Polarization Behavior. As seen from EIS presented in Figure 1, there is only one loop in the low overvoltage region. In such cases, the resistance R_p is usually associated with the charge transfer across the catalyst/electrolyte interface. However, if the time scale of the charge-transfer process is close to that of the diffusion processes responsible for the surface concentration of the electroactive species, R_p may contain contributions from all types of processes. Information on those contributions may be obtained from an analysis of the dependence of R_p on the cathode potential.

To establish whether the observed potential dependence reflects a pure kinetic control over the entire investigated potential range, or contains contributions due to the slow oxygen diffusion in the agglomerate, the cathode potential (*IR*-corrected cell voltage) was represented as a function of log R_p^{-1} (Figure 3). The R_p in this plot are values obtained for R_1 from NLSQ fitting of the equivalent circuits of Scheme 1b,c. If charge transfer is the only process responsible for R_p, the resulting Tafel plot is expected to be a straight line with an intercept E_o and a slope equal to $b = 2.3b'$, where $b' = RT/\alpha nF$, $\alpha \cong 0.5$, and n is the number of electrons transferred in the rate-determining step of the electrode process:

$$V_{cath} = E_o - b\ log\ R_p^{-1} \quad (4)$$

Figure 3 presents the plots obtained with two different humidification temperatures (31 and 60 °C). In both cases three potential ranges can be distinctly observed, for the potential dependence of the resistance: in the lowest overpotential range (cathode potentials higher than V_1) the slope of the straight line b_1 is close to 0.12 V/decade, as expected for a charge-transfer noncomplicated by diffusion processes. This value is similar with that obtained for the ORR (oxygen reduction reaction) in liquid electrolytes, but higher than that reported in previous studies[1,2] from resistance measurements.

The values of the parameters E_o and b_1, obtained from the linear plots in Figure 3, are presented in Table 1. From the intercept E_o and the value of the theoretical open circuit potential for oxygen reduction E_{eq} , the value of the specific charge-transfer resistance r_o at open circuit potential (OCP) may be evaluated:

$$E_o = E_{eq} - b \log R_o = E_{eq} - b \log r_o - b \log A \quad (5)$$

Here A is the total electrochemically active surface area, $A = Sa$, where S is the geometrical area and a is the electrochemically active area of the Pt electrocatalyst per unit of geometrical surface. The latter was determined for the electrode under investigation by cyclic voltammetry and was found to be 200 cm^2/cm^2. From r_o, an estimate of the exchange current density i_o may be obtained:

$$r_o = RT/nFi_o \quad (6)$$

TABLE 1: Fitting Parameters Obtained from the Tafel Plots for a GDE with a Pt/C Catalyst in a PEM Fuel Cell Operated at 25 °C with p_{H_2}/p_{Air} = 1 atm/1 atm[a]

t_h (°C)	E_o (V)	b_1 (V/decade)	b_2 (V/decade)	$10^{-4} r_o$ (Ω cm^2)	$10^6 i_o$ (A/cm^2)	R_p (Ω) (E_{cell} = 0.9 V)	R_p^* (Ω) (V_{cath} = 0.9 V)	C_{dl} (F) (E_{cell} = 0.9 V)
31	0.9435	0.123	0.250	1.91	1.34	0.4773	0.4438	0.3947
40	0.9501	0.131	0.271	1.32	1.93	0.4672	0.4148	0.3950
50	0.9516	0.134	0.263	1.10	2.32	0.4183	0.3806	0.3951
60	0.9616	0.134	0.278	0.63	4.06	0.4080	0.3475	0.3956

[a] Data are provided for different humidification temperatures t_h.

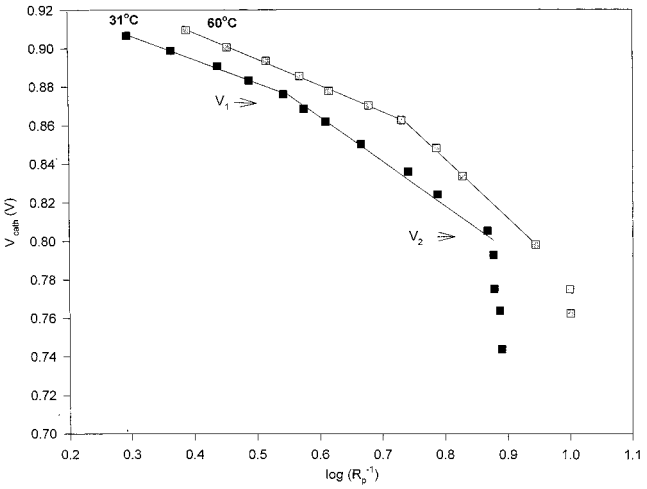

Figure 3. Cathode potential vs log(R_p^{-1}) at two humidification temperatures (31 and 60 °C). t_{cell} = 25 °C.

In (5), E_{eq} may be estimated for the conditions of the experiment, as a function of the molar fraction of the oxygen, corrected for the presence of liquid water in the humidified air.[23] The fraction of the latter x_{liq} can be evaluated from the difference of the partial pressures of water at the temperature of the cell (t_{cell}) and at the temperature of the humidifier (t_h).

$$E_{eq} = 1.23 + (RT/nF) \log p_{air}\, x_{O_2}/(1 - x_{liq}) \qquad (7)$$

The values of r_o and of the exchange current density i_o determined from (5)−(7) (Table 1) are in an excellent agreement with previous estimates.[5,7]

Table 1 also presents the values of the resistance and capacitance at the highest limit of the potential range (E_{cell} = 0.9 V) close to OCP, where mass transport effects are negligible.

At cathodic potentials in the range $V_1 < V < V_2$, a sudden doubling of slope (b_2) is observed in Figure 3. The values of b_2 obtained with different humidification temperatures are also presented in Table 1.

At potentials lower than V_2 the value of R_p remains practically constant and then starts increasing slowly. In the same range, a new loop appears in EIS at the lowest frequencies, the diameter of which (R_d) increases with decreasing voltage (Figure 1b). Due to this component, the total resistance $R_t = R_p + R_d$ starts increasing with decreasing voltage and the slope of the dependence V_{cath} vs log R_t^{-1} changes sign.

Discussion in Terms of the Flooded-Agglomerate Model. The potential dependence of the LF resistance for the ORR on GDE was analyzed in terms of the thin-film/flooded-agglomerate model of gas diffusion electrodes developed by Raistrick.[9,10] The physical basis of the model was presented in the introductory part. According to this model, the cathode catalyst layer is responsible for two types of mass transport limitations for ORR: (a) the progressive depletion of oxygen within a pore (agglomerate diffusion); (b) the diffusion of oxygen across an electrolyte layer of finite thickness at the catalyst surface (thin film diffusion). A simple diagnostic can be used to distinguish between the presence of agglomerate and thin film diffusion effects:[10] for the former, the low-frequency resistance decreases with increasing potential, while, for the latter, the opposite trend is observed.

The model enables deriving a simple equation for the reduced resistance R/R_o, where R was obtained from the low-frequency limit ($\omega \rightarrow 0$) of the EI spectrum:

$$R/R_o = 2(1 + \Gamma e^{\mu}\gamma)/[(\sigma + \gamma)e^{\mu}] \qquad (8)$$

Here μ is the ratio overpotential/slope of Tafel plot ($\mu = \eta_c/b'$), $\gamma = (\tanh \Phi\, e^{\mu/2})/(\Phi e^{\mu/2})$, $\sigma = \mathrm{sech}^2\, \Phi\, e^{\mu/2}$, and Φ is a parameter characterizing the agglomerate diffusion, while Γ defines the thin film diffusion:

$$\Phi = (k_o L_y/D_a)^{1/2} \quad \Gamma = (\delta k_o/D_f) \qquad (9)$$

Here L_y and δ are respectively the thickness of the catalyst layer and that of the electrolyte layer at the agglomerate surface and D_a and D_f are the diffusion coefficients of oxygen in the agglomerate and in the electrolyte film.

From (8) it is apparent that for very small values of μ, when γ approaches unity, the decrease of R_p with the overpotential has the simple expression presented in the preceding section:

$$R_p = R_{ct} = R_o e^{-\mu} \qquad (10)$$

At larger potentials, R_p depends on the relative magnitude of Φ and Γ. For $\Gamma = 0$, R_p continues to decrease with increasing overpotential, but the slope of the plot [V_{cath} vs log(R^{-1})] doubles, due to the potential dependence of the term ($\sigma + \gamma$):

$$R_p = 2R_o/[e^{\mu}(\sigma + \gamma)] \qquad (11)$$

Finally, at even larger potentials, when the term in Γ becomes nonnegligible, an additional resistance appears, due to thin film diffusion, which increases with increasing potentials.

With the criterion proposed by Raistrick, the experimental potential dependence of R_p in Figure 3 can be interpreted in terms of the existence of both agglomerate and thin film diffusion, even if there are no separate loops observed in EIS: a simple Tafel-type dependence of resistance as described by eq 10 at the lowest overpotentials, a doubling of slope in the intermediate potential range, where the current penetration in the agglomerate is incomplete (eq 11); finally, at the largest overpotentials, an apparent slope tending to infinity, showing that thin film diffusion becomes nonnegligible.[1] At cell potentials lower than 0.65 V, R_p starts increasing (Figure 1b), demonstrating that thin film diffusion becomes preponderant. The existence of a "turnaround potential", at which the HF loop starts increasing, was also observed by other authors.[1,2]

At cathodic potentials lower than V_2, the second (LF) loop appears in the spectrum and the impedance pattern becomes similar with that predicted by Raistrick for a system with thin film diffusion preceding the agglomerate process.[10] On the basis

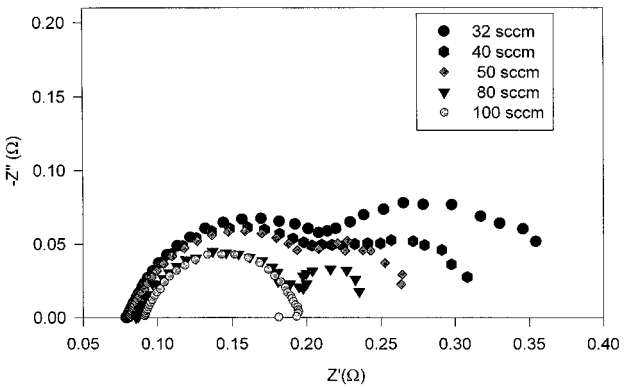

Figure 4. EIS spectra at 0.65 V with different air flow rates. $t_{cell} = 25$ °C, and $t_{H_2}/t_{air} = 40$ °C/40 °C.

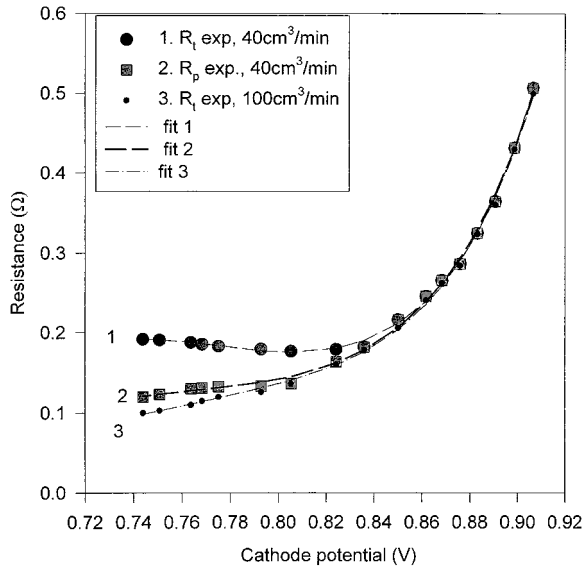

Figure 5. Experimental (points) and fitted (lines) potential dependence for the total resistance R_t at 40 cm^3/min (curve 1), catalyst layer resistance (R_p) (curve 2) at 40 cm^3/min, and R_t at 100 cm^3/min (curve 3).

of the flow rate dependence of EIS (Figure 4), which will be discussed below in more detail, we assigned this loop to the mass transport barrier in the backing, resulting as a consequence of water accumulation in this layer. Starting with the potential at which R_d appears, the total resistance ($R_t = R_p + R_d$) begins to increase with the overpotential. Figure 5 provides a comparison of the plots R_t and R_p vs V_{cath}, obtained in experiments with different air flows. It appears that at the higher flow rate (100 cm^3/min), R_t decreases continuously with V_{cath} (curve 3); at the lower flow rate (40 cm^3/min), R_t first decreases and then increases with decreasing V_{cath} (curve 1). For the former, the dependence of R_t is almost coincident with the dependence of R_p , obtained with a lower flow rate (40 cm^3/min, curve 2). Therefore, it may be concluded that, at higher flow rate, the new diffusional barrier responsible for R_d disappears and that this has little effect on the mass transport in the catalyst layer.

Equation 8 was used to fit the potential dependence of R_t at 40 cm^3/min (curve 1). The values of the fitted parameters are presented in Table 2. The fit could not distinguish between the two components due to thin film diffusion: in the Nafion film and in the backing. Therefore, one single parameter Γ was determined. However, a separation of the two components is still possible, by fitting the potential dependence of R_p, which is not influenced by the diffusion in the backing layer (fit 2 in

TABLE 2: Fitting Parameters for the Flooded Agglomerate Model

curve fitted	E_o (V)	b_1 (V/decade)	$10^{-4} r_o$ (Ω cm^2)	$10^4\Gamma$	Φ
1	0.9410	0.0859	15.6	1.16	0.204
2	0.9450	0.0945	5.90	0.71	0.274
3	0.9446	0.0965	6.62	0.61	0.324

Figure 5). As seen from Table 2, the parameter Γ thus determined is smaller than that obtained from the R_t fit and close to that obtained by fitting the dependence of R_t at 100 cm^3/min (curve 3).

Using the estimates for the various resistive components, the overpotential losses may be calculated at each potential. Figure 6 presents the results of such an estimate for a cell potential $E_{cell} = 0.65$ V.

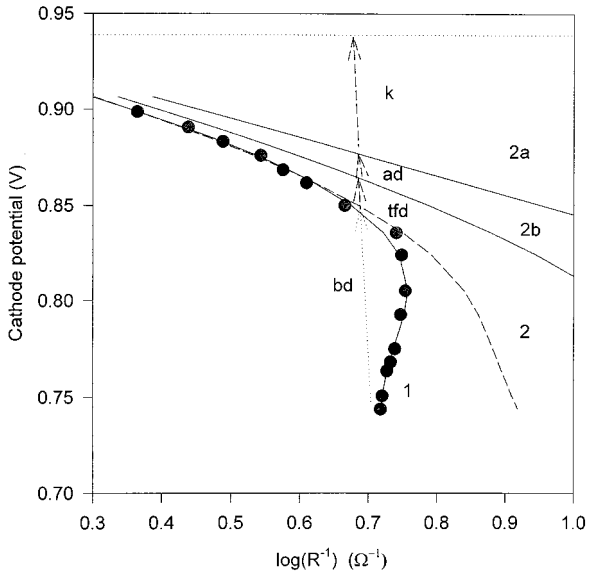

Figure 6. Estimated contributions of various terms to cathode overpotential losses: k, kinetic; ad, agglomerate diffusion; tdf, thin layer (Nafion at the catalyst surface); bd, diffusion in the backing.

This figure compares the contributions to the overpotential loss due to various effects: kinetic (k), agglomerate diffusion (ad), thin film diffusion in the Nafion layer (tfd). The corresponding contributions were obtained with the parameters evaluated from the fit of R_p: curve 2a was obtained by extrapolation of eq 10, and curve 2b, with eq 11. It may be seen that, when the component due to slow diffusion in the backing appears, it becomes the major source of overpotential loss.

Assignment of the LF Arc. Effect of Air Flow Rate on EIS. The assignment of the LF loop in EIS of PEM FC was an object of controversy, as discussed in the introductory part. Our data support the conclusion of Springer et al.,[1] who assigned it to oxygen diffusion limitations in the backing. The fact that R_d increases with the cathode overpotential shows that the LF loop is due to diffusion in a thin layer of finite thickness; i.e., it is a Nernst impedance. We could reproduce the experiments performed by Springer et al.,[1] demonstrating an important increase of R_d with the thickness of the carbon paper; such experiments show that R_d is due to flooding of the backing. The strong dependence of R_d on the flow rate (Figure 7) and the high values of R_d at low v_{air} reflect the appearance of a concentration gradient of oxygen in the backing, as a result of the decrease of effective porosity by accumulating water. Liquid water starts flooding the backing when the rate at which it accumulates (by electrochemical process, electroosmotic drag, and condensation

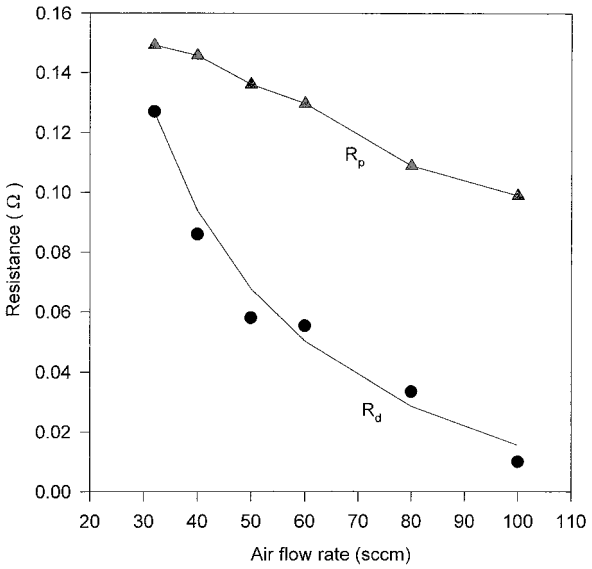

Figure 7. Dependence of R_d and R_p on air flow rate. Data were collected with a cell operated at $V_{cell} = 0.65$ V, $t_{cell} = 25$ °C, and $t_{H_2}/t_{air} = 40$ °C/40 °C.

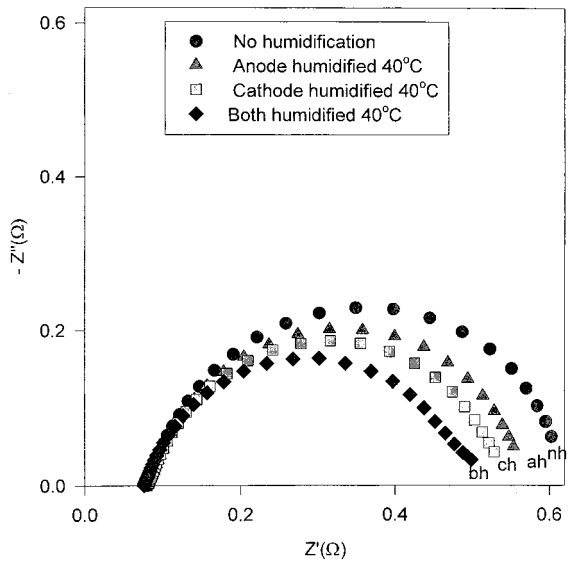

Figure 8. Effect of humidification type at $E_{cell} = 0.9$ V. Key: nh, nonhumidified; ah, anode-humidified, cathode bypass; ch, cathode-humidified, anode bypass; bh, both humidified. $t_{cell} = 25$ °C, and $\upsilon_{H_2}/\upsilon_{air} = 16$ sccm/40 sccm.

from the humidified air stream) becomes larger than that at which it is removed from the cathode (by back-diffusion through the membrane and evaporation in the air flow). The observed disappearance of the LF loop at high air flow rates may thus be explained by an acceleration of the removal of the accumulated water by evaporation.

Any factor capable of accelerating back-diffusion should produce the same trend: for example, this explains the positive effect of periodic purging of the anodic compartment, normally used when the fuel cell is operated with hydrogen in "dead-end" mode. Also, the same trend is expected when the thickness of the membrane is lowered; this explains why, in experiments reported by Paganin et al.,[2] the characteristic frequency of the LF loop shifts to higher frequencies as the thickness of the membrane is lowered.

According to Raistrick,[9,10] the agglomerate diffusion cannot produce a limiting current in the potential−current curves; the potential at which the limiting current appears is coincident with the change in the sign of slopes in the V_{cath} – log R_t^{-1} plot. At this potential, it is the competition between diffusion in the backing and that in the thin film of polymer that results in the appearance of a limiting current. The former is a very slow process, as results from inspection of the characteristic frequency of the LF curve, which is in the 0.065−0.1 Hz range. This frequency can be accounted for by a diffusion layer with a thickness of 0.025 cm and an effective diffusion coefficient of oxygen in the range $(6-4) \times 10^{-5}$ cm^2/s. On the contrary, diffusion in the thin Nafion layer is a relatively rapid process: a characteristic frequency for this process was estimated by Paganin et al.[2] to be in the 10^4 Hz range. Even if this value is overestimated, there is little doubt that the time scale for this process is much shorter than for diffusion in the backing layer. [The value estimated by Paganin et al.[2] represents actually an upper limit for the characteristic frequency: an effective diffusion coefficient in Nafion corrected for the tortuosity factor and the subunitary fraction of Nafion in the catalyst layer should be lower than assumed; the thickness assumed for the Nafion in the catalyst layer is lower than considered by most authors.] Therefore, slow diffusion in the backing determines the appearance of a limiting current long before the thin Nafion layer.

The strong dependence of R_d on the air flow rate provides an explanation for the fact that most reports on the EIS behavior of PEM FC did not reveal the presence of the second loop: in experiments with small cells, the air flow rate is generally much higher than the stoichiometric flow, which prevents cathode "overflooding". Also, this explains the great variability in the values of the reported potential for the appearance of R_d.

Effect of Humidification on EIS. The effect of moderate humidification on the EIS pattern was studied in various conditions over the entire investigated voltage range.

Figure 8 presents a typical EIS pattern at $E_{cell} = 0.9$ V in the absence of humidification (nh), with both compartments humidified (bh) and with a single compartment humidified—anodic (ah) or cathodic (ch). It may be observed that the values R_p decrease in the order: nh > ch > ah > bh. The trend is similar with that reported by Springer[1] at higher operating temperatures. Since the example is presented for the highest limit of the potential range, where there are no mass transport limitations, the observed trend can be assigned to the change value of R_o. There are two main reasons for this change. One is the fact the partial pressure of oxygen increases in (7) with the fraction of liquid water x_{liq}, which results in an increase of E_o. x_{liq} increases due to condensation, as the cathode compartment is humidified, and due to a decrease of back-diffusion of water, as the anode is humidified. Another reason could be the fact that the ohmic conductibility of Nafion in the catalyst layer (κ) increases with x_{liq}; according to Bockris,[24] the latter effect produces an increase in E_o, which is proportional with ln $\kappa^{1/2}$. In our experiments, both effects were small, since the operating temperature was low and the humidification was moderate. At higher cell temperatures, the dehydration of the nonhumidified membrane is more important; this explains why, in such conditions, differences reported by other authors[1] between humidified and nonhumidified cell were more important than those found in the present work.

Figure 9 presents comparatively the values of R_p obtained at various cell voltages. It may be observed that the effect of humidification is higher at high cell potentials (low overvoltage). In this range, R_p values decrease in the order nh > ah ≥ ch > bh. As the overvoltage increases, the diameters of the HF loop approach a common value and subsequently reverse the trend, showing that thin film diffusion becomes preponderant. For the LF loop the value of R_d increases in the order nh < ah < ch <

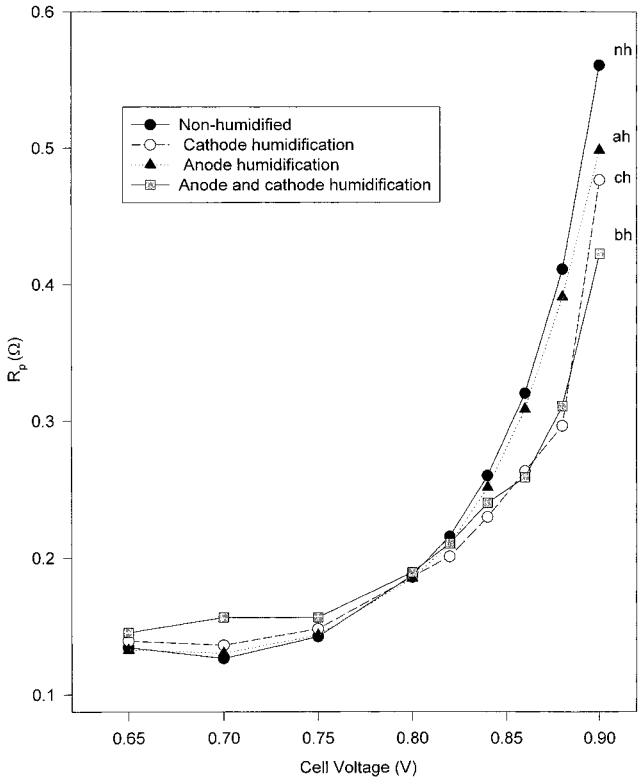

Figure 9. Effect of humidification on R_p at different cell voltages. Key: nh, nonhumidified; ah, anode-humidified, cathode bypass; ch, cathode-humidified, anode bypass; bh, both humidified. $t_{cell} = 25$ °C, and $v_{H_2}/v_{air} = 16$ sccm/40 sccm.

bh, which is expected if the mass transfer barrier responsible for this loop is assigned to presence liquid water in the backing of the cathode. However, both the relative and absolute changes are small, which shows that, in the conditions of the experiment, most of the water accumulated in the backing results from the electrochemical process.

Another series of experiments was performed by changing the humidification temperature, with both compartments humidified. The observed changes were presented in Figure 10 in a tridimensional diagram. It may be seen that at high cell potentials (low cathodic overvoltage), the value R_p shows a progressive decrease with increasing humidification temperature. The differences between values obtained at various humidification temperatures decrease with increasing cathodic overvoltage, and at the lower limit of the investigated voltage interval, the R_p values become almost identical. On the contrary, for the LF loop, the R_d values show a moderate increase with increasing temperature, a trend which can be easily explained in terms of the increase of the amount of liquid water resulting from condensation in the pores of the backing (Figure 11).

The dependencies V_{cath} vs $\log(R_p^{-1})$ were recorded for four values of the humidification temperatures in the 30−60 °C range. The plots at the extremes of this range are those presented in Figure 3. The values of the slopes of the plot for the four humidification temperatures, as well as the values i_o and r_o, which characterize the apparent electrode activity in the conditions of the experiment, were presented Table 1. The values obtained show an apparent increase of i_o with the humidification temperature. Since r_o results from an extrapolation, a more simple criterion to compare charge-transfer resistances is to use the experimental values of R_p at $E_{cell} = 0.9$ V or, better, at $V_{cath} = 0.9$ V. In Table 1, the latter values, denoted by R_p* were

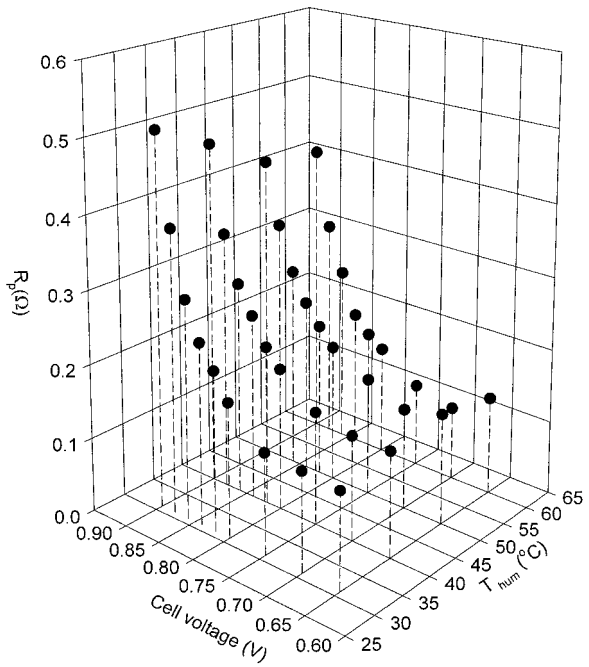

Figure 10. Dependence of R_p on humidification temperature at different cell voltages. $t_{cell} = 25$ °C, and $v_{H_2}/v_{air} = 16$ sccm/40 sccm.

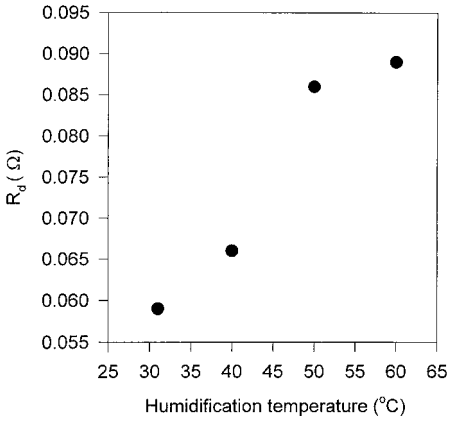

Figure 11. Dependence of R_d on humidification temperature. $E_{cell} = 0.65$ V, $t_{cell} = 25$ °C, and $v_{H_2}/v_{air} = 16$ sccm/40 sccm.

evaluated at $V_{cath} = 0.9$ V, using the fitted parameters of E_o and b.

Table 1 also presents the values of double layer capacitance (C_{dl}) evaluated from the experimental values T_{dl} at $E_{cell} = 0.9$ V. Unlike the R_o values, the values C_{dl} do not show important changes with the humidification temperature, which indicates that there is no change in the electrochemically active surface area.

Conclusions

EIS studies on PEM fuel cells demonstrate the potentialities of this method as a tool for investigating electrode processes and for the characterization of the influence of operating conditions. The impedance spectra of H_2/air PEM fuel cells were investigated at room temperature, and their voltage dependence was examined as a function of humidification and air flow rate. The major advantage of the EIS method with respect to steady-state measurements is the capacity to separate the individual contributions of components to the overall cell impedance:

(a) One component is the ohmic resistance of the membrane, which can be estimated from the HF limit of the spectrum.

(b) Another component is the impedance of the cathode catalyst layer, responsible for the appearance of a loop in the medium frequency domain. An analysis of the voltage dependence of EIS in terms of the flooded-agglomerate model enabled separating the effects due to charge transfer, air diffusion through the transversal pores of the catalyst layer, and diffusion in the Nafion layer surrounding the catalyst particles. The cathode parameters determined by fitting the experimental voltage dependence to the model predictions are in agreement with those obtained from steady-state measurements.

(c) A final component is the impedance of the cathode backing, responsible for a low-frequency loop in the spectrum, which increases with increasing cathode overvoltage. This loop appears once the liquid water produced at the cathode starts to accumulate in the backing, resulting in a limitation of the air transport to the backing/catalyst layer interface. Once the backing starts being overflooded by liquid water, the contribution of this effect to the cathode impedance becomes dominant and represents the major cause of current limitation at low cell voltage.

A further advantage of the EIS method as a diagnostic tool for fuel cell investigation is that it enables one to study separately the effect of operating conditions on the fuel cell components. Thus, it was demonstrated that increasing the air flow rate produces a rapid decrease of the impedance due to cathode backing, but has little influence on the catalyst layer. On the contrary, improvement of the humidification produces a decrease of the impedance due to the catalyst layer, probably due to an increase of the conductibility of the Nafion in this layer.

Acknowledgment. The authors gratefully acknowledge the contribution of Dr. A. Attia of H Power Corp. and thank him for the careful revision of the manuscript.

References and Notes

(1) Springer, T. E.; Zawodinski, T. A.; Wilson, M. S.; Gottesfeld, S. *J. Electrochem. Soc.* **1996**, *143*, 587.
(2) Paganin, C.; Oliveira, C. L. F.; Ticianelli, E. A.; Springer, T. E.; Gonzales, E. R. *Electrochim. Acta* **1998**, *43*, 3761.
(3) Wagner, N.; Schnurnberger, W.; Müller, B.; Lang, M. *Electrochim. Acta* **1998**, *43*, 3785.
(4) Okada, T.; Xie, G.; Tanabe, Y. *Electroanal. Chem.* **1996**, *413*, 49.
(5) Ciureanu, M.; Wang, H. *J. Electrochem. Soc.* **1999**, *146*, 4031.
(6) Ciureanu, M.; Wang, H.; Qi, Z. *J. Phys. Chem.* **1999**, *103*, 9645.
(7) da Silva, S. L. A.; Ticianelli, E. *J. Electroanal. Chem*. **1995**, *391*, 101.
(8) Lee, S. J.; Mukerjee, S.; McBreen, J.; Rho, Y. W.; Kho, Y. T.; Lee, T. H. *Electrochim. Acta* **1998**, *43*, 3693.
(9) Springer, T. E.; Raistrick, I. D. *J. Electrochem. Soc*. **1989**, *136*, 1594.
(10) Raistrick, I. D. *Electrochim. Acta* **1990**, *25*, 1579.
(11) Dirard, J. P.; Le Gorec, B.; Montella, C. *J. Power Sources* **1998**, *70*, 78.
(12) Bultel, Y.; Ozil, P.; Durand, R.; Simonsson, D. *Electrochem. Soc. Proc*. **1995**, *95*−*23*, 43.
(13) Perez, J.; Tanaka, A.; Gonzalez, E. R.; Ticianelli, E. A. *J. Electrochem. Soc.* **1994**, *141*, 431.
(14) Giner, J.; Hunter, C. *J. Electrochem. Soc.* **1969**, *116*, 1124.
(15) Gloaguen, F.; Convert, P.; Gambuzorzev, S.; Velev, O. A.; Srinivanasan, S. *Electrochim. Acta* **1998**, *43*, 3767.
(16) Ticianelli, E. A. *J. Electroanal. Chem.* **1995**, *387*, 1.
(17) Dirard, J. P.; Le Gorec, B.; Landaud, P.; Montella, C. *Electrochim. Acta* **1997** *42*, 3417.
(18) Lasia, A. In *Modern Aspects of* Electrochemistry; Conway, B. E., Bockris, J. O. M., White R. E., Eds.; Plenum: New York, 1999; Vol. 32, p 143.
(19) McHardy, J.; Baris, J. M.; Stonehart, P. *J. Appl. Electrochem.* **1975**, *6*, 371.
(20) Holze, R.; Vielstich, W. *J. Electrochem. Soc.* **1984**, *131*, 2298.
(21) Springer, T.; Wilson, M. S.; Gottesfeld, S. *J. Electrochem. Soc.* **1993**, *140*, 3513.
(22) Ciureanu, M. Unpublished results.
(23) Springer, T. E.; Zawodinski, T. A.; Gottesfeld, S. *J. Electrochem. Soc.* **1991**, *138*, 2334.
(24) Bockris, J. O. M.; Srinivanasan, S. *Fuel Cells. Their Electrochemistry*; McGraw-Hill: New York, 1968.